BBA - Bioenergetics 1860 (2019) 591–599

Contents lists available at ScienceDirect

BBA - Bioenergetics

journal homepage: www.elsevier.com/locate/bbabio

Single-molecule study of redox control involved in establishing the spinach plastocyanin-cytochrome b_6f electron transfer complex

Guy E. Mayneord, Cvetelin Vasilev, Lorna A. Malone, David J.K. Swainsbury, C. Neil Hunter, Matthew P. Johnson*

Department of Molecular Biology and Biotechnology, University of Sheffield, Firth Court, Western Bank, Sheffield S10 2TN, United Kingdom

ARTICLE INFO

Keywords:
Photosynthesis
Electron transfer, cytochrome *b6f*
Plastocyanin
Atomic force microscopy

ABSTRACT

Small diffusible redox proteins play a ubiquitous role in bioenergetic systems, facilitating electron transfer (ET) between membrane bound complexes. Sustaining high ET turnover rates requires that the association between extrinsic and membrane-bound partners is highly specific, yet also sufficiently weak to promote rapid post-ET separation. In oxygenic photosynthesis the small soluble electron carrier protein plastocyanin (Pc) shuttles electrons between the membrane integral cytochrome b_6f (cytb_6f) and photosystem I (PSI) complexes. Here we use peak-force quantitative nanomechanical mapping (PF-QNM) atomic force microscopy (AFM) to quantify the dynamic forces involved in transient interactions between cognate ET partners. An AFM probe functionalised with Pc molecules is brought into contact with cytb_6f complexes, immobilised on a planar silicon surface. PF-QNM interrogates the unbinding force of the cytb_6f-*Pc* interactions at the single molecule level with picoNewton force resolution and on a time scale comparable to the ET time in vivo (ca. 120 µs). Using this approach, we show that although the unbinding force remains unchanged the interaction frequency increases over five-fold when Pc and cytb_6f are in opposite redox states, so complementary charges on the cytb_6f and Pc cofactors likely contribute to the electrostatic forces that initiate formation of the ET complex. These results suggest that formation of the docking interface is under redox state control, which lowers the probability of unproductive encounters between Pc and cytb_6f molecules in the same redox state, ensuring the efficiency and directionality of this central reaction in the '*Z*-scheme' of photosynthetic ET.

1. Introduction

Photosynthetic and respiratory electron transfer (ET) reactions sustain virtually all life on Earth. Small, water-soluble redox proteins play a ubiquitous role in biological ET by shuttling electrons between generally larger membrane integral redox complexes [1]. The interactions between the soluble protein and its membrane-bound partner must balance conflicting requirements: they must be highly specific to facilitate efficient ET, yet they must also be sufficiently weak to allow rapid post-ET separation in order to sustain a high turnover rate (reviewed in [2,3]). Somehow therefore, the forces that brought the ET complex together initially must be reversed following the sub-millisecond ET event to ensure their rapid dissociation, yet how this is achieved remains poorly understood [3]. One particularly well studied small diffusible redox protein is plastocyanin (Pc), found in oxygenic photosynthetic systems in cyanobacteria, plant and algal chloroplasts, which transfers electrons from cytochrome b_6f (cytb_6f) to photosystem I (PSI) (reviewed in [2,4]). The redox active co-factor in Pc is a copper atom, which cycles between +1 and + 2 oxidation states [5]. Pc accepts an electron from the *c*-type haem of cytochrome *f* and delivers it to the P700 special-pair chlorophylls of PSI. To achieve this transfer, oxidised Pc must diffuse over distances up to 250 nm between these two membrane integral complexes, through the narrow (ca. 10 nm wide) protein-crowded thylakoid lumen [6,7].

Most current models suggest that soluble redox proteins and their membrane integral partners associate in a stepwise manner, with the first step involving an initial encounter complex steered by long-range electrostatic interactions. The encounter complex is generally thought to be the prelude to the formation of the productive or active ET complex in which short-range hydrophobic interactions between aromatic and non-polar residues surrounding the redox co-factor binding sites are important [8,9]. The effect of the encounter complex is to bring the ET partners together in an orientated state that minimises the number and scale of rotational and translational movements of the partners required to find the optimum conformation for productive ET [3]. Factors that sustain rapid ET have been investigated by structural

* Corresponding author.
E-mail address: matt.johnson@sheffield.ac.uk (M.P. Johnson).

https://doi.org/10.1016/j.bbabio.2019.06.013
Received 1 April 2019; Received in revised form 18 June 2019; Accepted 21 June 2019
Available online 24 June 2019
0005-2728/

and mutational studies, which have highlighted the importance of complementary electrostatic interactions between the acidic patch of residues on Pc (D42, E43, D44, E45, E59, E60, D61) and a basic patch of residues on cyt *f* (K58, K65, K66 and K187), as well as hydrophobic patches surrounding both the haem and copper cofactors on cyt *f* and Pc, respectively [2,10–15]. The importance of the encounter complex for ET rates is readily demonstrated by their dependence on the ionic strength of the aqueous medium (e.g. [11,16,17]). At high ionic strength the ET rate declines since the attractive electrostatic interactions are screened. Nuclear magnetic resonance (NMR) studies of biological ET complexes show that the encounter complexes are characterised by very small chemical shift perturbations spread out over relatively large areas of the proteins; thus, the interactions that establish ET complexes are highly dynamic and lack a single well-defined organisation, with the electrostatic interactions remaining fully-solvated and any salt-bridges being mediated by intervening water molecules [15,18–21]. Molecular dynamics simulations of the cytochrome c_2 (cytc_2) - cytochrome bc_1 (cytbc_1) interaction similarly suggest a 'fuzzy' encounter complex with multiple conformational states that bring the redox co-factors into close proximity [22]. Moreover, this study suggested that the majority of the stored redox energy is expended on partner recognition and binding rather than on driving electron transfer [22].

While the ensemble studies described above have been useful in defining the general characteristics of ET complexes, the averaging involved obscures the heterogeneity inherent within the system. Ideally it would be possible to quantify the forces involved in the putative encounter and productive complexes at the single-molecule level and to understand their temporal, ionic strength and redox dependence. Recently, we used the pico-Newton force sensitivity and nanometre spatial resolution of the AFM, specifically PF-QNM, to quantify the unbinding force between the soluble redox protein cyt c_2 attached to the scanning probe and its ET partner, the reaction centre (RC) - light harvesting 1 (LH1) complex from *Rhodobacter (Rba.) sphaeroides* immobilised on a gold substrate [23]. In another such PF-QNM study we mapped the organisation of the cytb_6f complex in spinach thylakoids using its interaction with Pc attached to the AFM probe as a spatial marker [24]. However, the statistics of this latter study were necessarily limited by the relatively small number of membrane-embedded cytb_6f molecules that could be measured. In the present study we use purified, surface-immobilised cytb_6f complexes, which allowed a more detailed investigation of the redox and salt dependence of the Pc-cytb_6f interaction at the single-molecule level.

2. Results

2.1. Single molecule force spectroscopy of the interaction between cyt b_6f and Pc

Pc and dimeric cytb_6f complexes were purified from spinach (see Supplementary Figs. 1–3). For these experiments the cytb_6f was pre-reduced using sodium ascorbate and Pc was pre-oxidised using potassium ferricyanide. The dimeric cytb_6f complexes were immobilised on a SiOx substrate functionalised with (3-mercaptopropyl)trimethoxysilane (MPTMS) and attached via the short linker sulfosuccinimidyl 4-(*N*-maleimidomethyl)cyclohexane-1-carboxylate (SMCC) (Supplementary Fig. 4A). Purified Pc was attached to an AFM probe covered in a MPTMS monolayer, using a heterobifunctional 10 nm-long polymer linker SM $(PEG)_{24}$, terminated with *N*-hydroxysuccinimide ester (NHS) for reaction with primary amines (lysines) on the surface of Pc (Supplementary Fig. 4B). The crystal structure of spinach Pc [25] reveals that 6 lysine residues (K30, K54, K71, K77, K81 and K95) are available to form covalent NHS-ester linkages with the functional monolayer on the AFM probe, all of which are distal to the Cu-containing active site; thus, coupling of Pc to the AFM probe is unlikely to prevent binding to cytb_6f (see Supplementary Fig. 5). In the PF-QNM experiment the Pc-functionalised probe is brought into contact with the cytb_6f molecules on the surface, whereupon a specific interaction can occur; subsequently the upward movement of the probe fully extends the flexible linker before rupturing the interaction (Fig. 1A). The distribution of immobilised

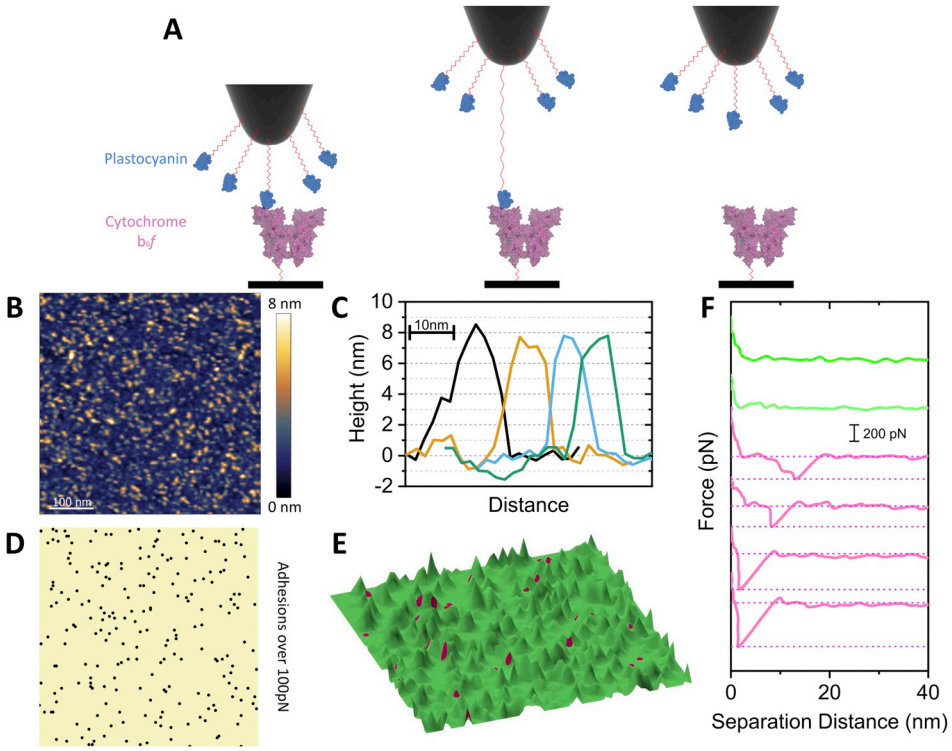

Fig. 1. Single molecule force spectroscopy of the interaction between cytb_6f immobilised on a SiOx surface and Pc attached to the AFM probe. (A) Cartoon depicting the principle of the PF-QNM experiment. The AFM probe, functionalised with Pc proteins attached via a flexible 10-nm-long SM $(PEG)_{24}$ linker, laterally images the topography of the *cytb_6f* complexes immobilised on a SiOx substrate via a tapping motion, while simultaneously recording probe-sample unbinding forces for every pixel. In the first panel one of the Pc proteins attached to the AFM probe binds to a cytb_6f complex on the surface; in the second panel the flexible linker is extended to its full 10 nm length as the AFM probe is withdrawn from the surface during the upward part of the tapping motion; in the third panel the force applied has exceeded the protein interaction force and has ruptured the Pc-cytb_6f interaction. (B) AFM topograph showing the distribution of cytb_6f complexes on the SiOx surface. (C) Examples of height profiles of individual cytb_6f complexes; the measured height is ca. 8.0 nm. (D) AFM adhesion image showing areas where adhesion exceeds 100pN; this comprises both specific or non-specific interactions. (E) 3D rendering of a subsection (250 × 250 nm) of the AFM height and adhesion data, reveals a coincidence between the regions of high unbinding force (pink) and the protrusions corresponding to cytb_6f molecules. (F) Examples of force-distance curves representing no interaction (green, top two curves), specific interaction (pink middle two curves) and non-specific interaction (pink, bottom two curves). See results description for details.

cytb_6f complexes on the SiOx substrate is shown in the AFM topology image in Fig. 1B, as imaged in 10 mM HEPES pH 7.4, 5 mM NaCl and 0.05% glyco-diosgenin (GDN). The average 8.0 nm height (Fig. 1C) is consistent with the expected size of the cytb_6f complex [26]; the lateral dimensions are larger than expected based on the structure due to geometrical tip-convolution effects. The interactions between the cytb_6f complexes on the substrate and Pc on the probe are visualised in the simultaneously recorded adhesion image (Fig. 1D), which shows the locations of unbinding forces required to rupture the probe-surface interactions. The density of cytb_6f on the surface is ca. 430 per 500 × 500 nm scan window and the pixel density was 128 × 128; given that each pixel covers ca. 4 nm and the ~11 × 8 nm dimensions of cytb_6f (Fig. S3C), each complex would be contacted roughly 9–12 times during the imaging process). The force-curve repetition rate was 0.5 KHz for these experiments, which corresponds to a dwell-time of the AFM probe on the surface of ca. 500 μs, slightly longer than the cytb_6f -Pc ET time of 70–130 μs [5,27]. Overlaying the topographic (Fig. 1B) and adhesion images (Fig. 1D) reveals a good correlation between the points on the image where high unbinding forces are recorded (pink) and the 8 nm topographic features that correspond to immobilised cytb_6f complexes (Fig. 1E). The slight offset of the high adhesion force events from the centre positions of the cytb_6f complexes most likely result from interaction with Pc molecules attached with an offset (i.e. not directly at the apex) to the AFM probe, together with a scan direction artefact during the image acquisition. We were able to quantify these interactions by extracting and analysing the actual force-distance data obtained for each pixel of the adhesion image (see Materials & methods section). Fig. 1F shows examples of force-distance curves extracted from Fig. 1E; the top two curves (green) are representative of the vast majority of pixels in the image where we observe low unbinding forces comparable to the noise level of the measurement. The middle two force-distance curves in Fig. 1F (shown in pink) are recorded for some of the pink pixels in Fig. 1E. These curves show a large increase in the unbinding force (250-300pN) centered on a probe-sample separation distance of 10 nm, which indicates that the flexible linker attaching Pc to the probe is fully extended before interaction is ruptured, indicating a specific Pc- cytb_6f unbinding event. In contrast, the bottom two curves in Fig. 1F are recorded on the SiOx surface that lies in between cytb_6f complexes. They show a similarly high unbinding force but importantly at a probe-sample separation distance close to 0 nm, indicating a non-specific interaction between the bulk surface of the probe and the SiOx surface. This type of analysis allowed us to use the probe-sample separation distance as a selection criterion and to pool only the data specifically related to the interaction between cytb_6f complexes and Pc on the probe [24]. Each dataset was statistically analysed to evaluate the frequency of the occurring interaction events (interaction frequency) as well as the most probable unbinding force (see Materials and methods).

Fig. 2A presents a detailed statistical analysis of the distribution of the unbinding forces for over 6000 separate events, centered on a 10 nm probe sample-separation distance. To further verify that these represent specific Pc-cytb_6f unbinding events we tested the effect of saturating the available binding sites on the surface immobilised cytb_6f complexes by injecting free oxidised Pc into the AFM liquid cell at a final concentration of 90 μM, several times higher than the reported K_D of 25 μM [16]. After approximately 5 min incubation with free Pc new data were recorded with the same imaging parameters. Analysis of the data obtained before and after the blocking of the docking site revealed a nearly 4-fold lower frequency for interaction between the cytb_6f complex and the Pc attached to the AFM probe (Fig. 2B), but that the distribution of unbinding forces was unaffected (Fig. 2A). Given the 25 μM K_D and 90 uM concentration of added Pc, the blocking control still allows residual binding events. A similarly lowered interaction frequency was found previously for the excess Pc control used for the PF-QNM study of cytb_6f in grana membranes [24].

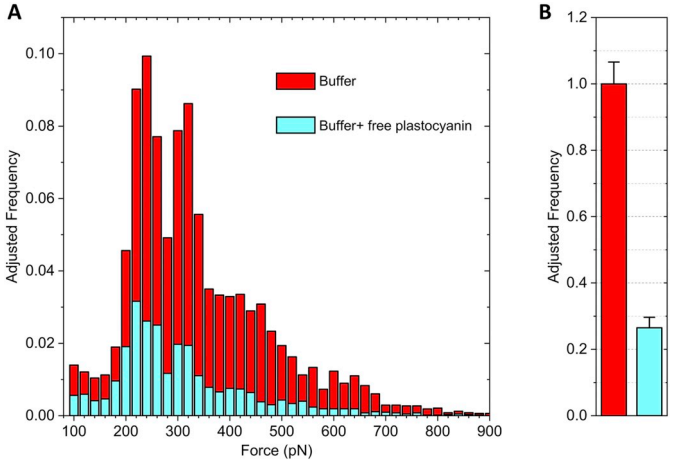

Fig. 2. Distribution of unbinding forces for the Pc-cytb_6f interaction and effect of free Pc (A) Distribution of forces measured for probe-sample separation distances centered on 10 nm, in the presence (cyan) and absence (red) of 90 μM free Pc in the imaging buffer. The cumulative frequency of each histogram was adjusted to reflect the interaction frequency plotted in (B), giving the adjusted frequency. (B) Mean frequency for the number of interactions observed between cytb_6f and Pc in the presence (cyan) and absence (red) of 90 μM free Pc in the imaging buffer. Frequency adjusted to buffer sample being a value of 1. Error bars show the standard error of the mean.

2.2. Changes in binding dynamics between different redox states

Having established that the unbinding events centered on a 10 nm probe-sample separation distance correspond to *bone fide* Pc-cytb_6f interactions, we next assessed the effect of the redox state of the partners by prior incubation with either sodium ascorbate (to reduce) or potassium ferricyanide (to oxidise). To ensure differences in probe preparation did not affect the interaction frequency (e.g. a probe with more Pc attached giving a higher interaction frequency), the initial experiment of reduced cytb_6f – oxidised Pc (cytb_6f[red] – Pc[ox]) was performed for 5 images, followed by a change in redox state to the given condition. The adjusted frequency was thus a comparison of the new condition to the cytb_6f[red] – Pc[ox]. Four different experiments were conducted where cytb_6f — Pc were either in complementary redox states; reduced cytb_6f – oxidised Pc (cytb_6f[red] – Pc[ox]) and cytb_6f [ox] – Pc[red], or in the same redox state; cytb_6f[ox]–Pc[ox] and cytb_6f [red] –Pc[red]. Fig. 3A compares the cumulative binding frequencies for all four redox pairs. It is evident that when the cytb_6f and the Pc are in the same redox state, the interaction frequency is substantially lower (by a factor of ca. 5) compared to the cytb_6f[red] – Pc[ox] pair, in qualitative agreement with our previous findings on membrane-bound cytb_6f [24]. The results for the 'post ET' state, cytb_6f[ox] – Pc[red], showed an equally high (within experimental error) interaction frequency. Due to the low driving force (30 mV, [5]) for electron transfer in this complex the similar interaction frequencies for cytb_6f[ox] – Pc [red] and cytb_6f[red] – Pc[ox] likely reflect the reversible electron transfer between tip-attached Pc and surface-attached cytb_6f during the dwell time of the tip on the cytb_6f complex. In addition the unbinding force distributions presented in Fig. 3B — E also show that the unbinding forces present in the pre-ET (cytb_6f[red] – Pc[ox]) and post-ET (cytb_6f[ox] – Pc[red]) states were nearly identical, both displaying two lower populations, with most probable unbinding forces (taken from the mean of Gaussian fitting) of 219 ± 64 pN and 311 ± 72 pN for cytb_6f[red] – Pc[ox], and 223 ± 63 pN and 313 ± 47 pN for cytb_6f [ox] – Pc[red]. The higher harmonics at ca. 400 and ca. 650 pN in Fig. 3B,C represent simultaneous unbinding events between two separate Pc molecules on the probe binding to two binding sites on the cytb_6f on the surface (either both sides of the dimer or two independent cytb_6f complexes), which is much less likely than individual unbinding

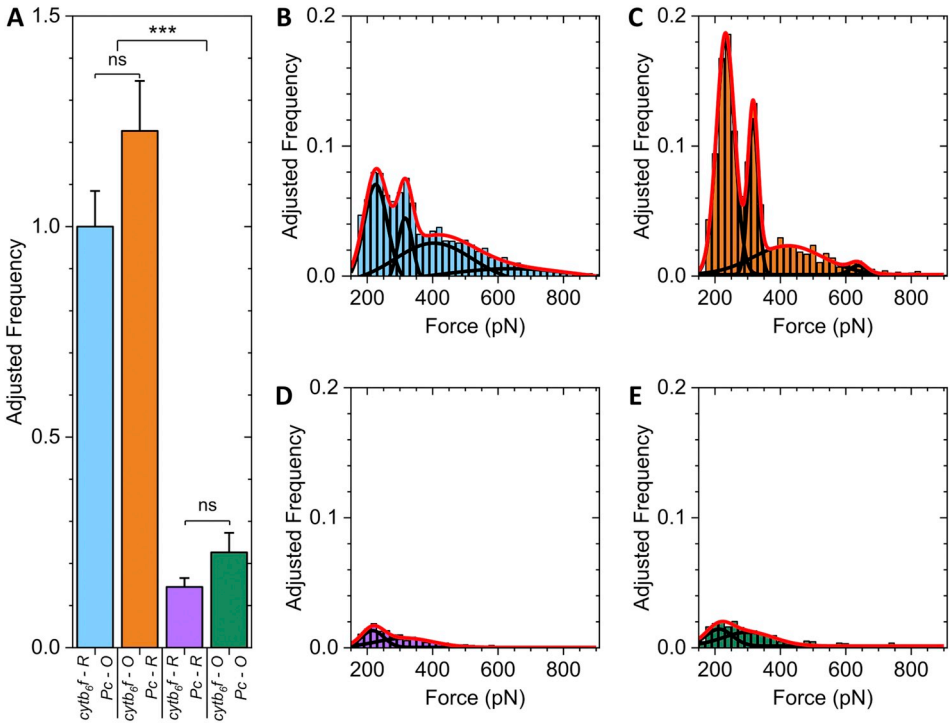

Fig. 3. Redox dependence of the interaction between cytb_6f and Pc. (A) Mean cumulative frequency for the interaction at different redox states (O – Oxidised, R – Reduced) represented as a bar chart. Adjusted frequencies represent the total number of interactions occurring, adjusted to the pre-ET transfer state (cytb_6f[red], Pc[ox]), error bars are standard errors of the mean. (B-E) Force distributions (most probable forces obtained from the Gaussian fits, red curves) for the interaction between; (B) cytb_6f[red] – Pc[ox], (C) cytb_6f[ox] and Pc[red], (D) cytb_6f[red] –Pc [red], and (E) cytb_6f[ox]–Pc[ox]. For each, the total area of the histogram reflects the adjusted frequency seen in (A). For B-E, the red line on each plot shows the multiple peak fitting Gaussian for the plot, and the black lines show the underlying single peak fits comprising the multipeak fit.

events given the low density of cytb_6f complexes on the surface and of Pc on the probe. Differences observed in the distribution of forces between pre and post ET states are simply the result of different distributions between single and double events. The forces observed for the cytb_6f[red] –Pc[red] and cytb_6f[ox]–Pc[ox] states are similar - 216 ± 68 pN and 314 ± 170 pN, and 212 ± 81 pN and 301 ± 155 pN, respectively, but the probability of such interactions is ca. 5 fold lower than for complementary redox pairs (Fig. 3D,E). The higher of the two interaction forces for ET partners in the pre-and post-ET states (311 ± 72 pN and 313 ± 47 pN, respectively) corresponds well with our previous study on cytb_6f in the grana membrane [24], which found a single most probable force of 312 ± 5pN. The present study identifies another probable unbinding force at a lower value (ca. 220 pN).

2.3. Effect of ionic strength on interaction frequency

In order to investigate the origin of the two unbinding forces (ca. 220 pN and ca. 310 pN) further, we measured the interaction of cytb_6f [red] –Pc[ox] as a function of the ionic strength of the medium. It has been shown previously that the initial steering and formation of the encounter complex is determined by several long-range electrostatic interactions [2,10–13]. In the context of our PF-QNM experiments increasing the dielectric constant of the surrounding medium (the imaging buffer in our experiments) should lead to a decrease of the interaction frequency due to a decrease of the Debye length, which in this case reflects the extent of the electrostatic effect exerted by the charged residues at the surfaces of cytb_6f and Pc. Such an experiment could also provide some more information on the bimodal distribution of unbinding forces, for example in Fig. 2A; it is possible that the lower ca. 220 pN peak represents the encounter complex where electrostatic interactions dominate, while the ca. 315pN peak represents the more tightly bound productive ET complex where hydrophobic interactions may further stabilize the complex in addition to the electrostatics. Thus, a range of salt concentrations could help to discriminate between two binding states.

We conducted a series of PF-QNM measurements using the cytb_6f [red] – Pc[ox] combination, while varying the ionic strength of the imaging buffer by increasing the salt concentration from the initial value of 5 mM NaCl up to 250 mM NaCl, thus covering a broader range than the physiologically relevant of salt concentrations (100–200 mM according to Izawa and Good [33]; Staehelin [34]). We note however that there appear to be no reports that measure the ionic strength of the lumenal space occupied by Pc in vivo. Interestingly, the ratio of the ca. 310 pN and ca. 220 pN peaks in the distribution of unbinding forces histogram in Fig. 4A remained broadly unchanged (following One-way ANOVA examination) over the entire range of salt concentrations, but the interaction frequency decreased significantly at higher salt concentrations (> 50 mM NaCl). This trend is evident in Fig. 4B, where the frequency of interaction is plotted against the salt concentration and the data follow an exponential decay. At the highest concentration of 250 mM NaCl the interaction frequency is decreased by a factor of ca. 5. Since similar pattern was observed for both force populations, the results suggest that the lower force peak is unlikely to arise specifically from the encounter complex.

2.4. Influence of the surface immobilisation chemistry and comparison to cytb_6f in native grana membranes

To find out if the immobilisation chemistry might exert an influence on the measured unbinding forces, in particular the presence of two peaks in the unbinding force histograms, we performed control experiments where the *cytb_6f* complexes were immobilised on a different substrate, epitaxial gold, using a thiol-based chemistry (Supplementary Fig. 4C). This new substrate and attachment chemistry, and the use of mixed monolayers, allowed more control over the surface density of the immobilised molecules. The surface density of the *cytb_6f* complexes on the functionalised epitaxial gold surface was found to be in the range 200–300 molecules per μm^2. A topography image (Fig. 5A) was recorded at a modulation frequency of 0.5 kHz, in imaging buffer (0.05% GDN, 45 mM KCl, 10 mM HEPES pH 7.4) and individual cytb_6f complexes can be clearly seen on the gold substrate with an average height of around 8 nm (Fig. 5B), consistent with the expected size of the cytb_6f complex [26] and taking into account convolution effects arising from the larger radius of curvature of the functionalised AFM probe. Fig. 5C shows the distribution of unbinding forces for the cytb_6f[red]- Pc[ox] interaction. This combination again gave a bimodal distribution of

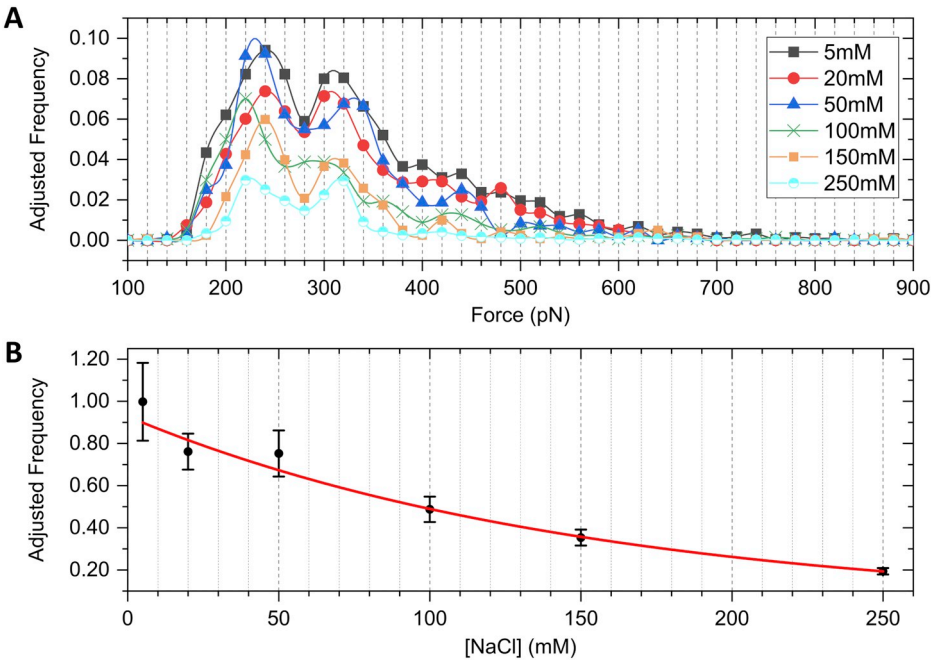

Fig. 4. Effect on unbinding forces and interaction frequency of varying ionic strength (A) Multiple overlaid histograms representing the distributions of unbinding forces for separating cytb_6f[red] – Pc[ox] measured at different salt concentrations, with the cumulative sum adjusted relative to 5 mM NaCl being 1. (B) Interaction frequency of each salt concentration adjusted relative to 5 mM NaCl being 1. Error bars display the standard error of the mean.

unbinding forces, with the most probable forces of 204 ± 49 pN and 307 ± 175 pN. The forces observed for the cytb_6f[red] –Pc[red] combination, Fig. 5D, were 212 ± 107 pN and 321 ± 62 pN, while the interaction frequency decreased by a factor of 3. All these results are consistent with the results obtained on SiOx substrates.

Another possible explanation for the presence of the peak at ca. 220 pN could be the orientation of the cytb_6f complex when immobilised on the substrate. In the experiments described so far, for Figs. 1–5, lysine side chains were used to tether the cytb_6f complex to the sample surface. This method lacks specificity in terms of presenting the lumenal face of the complex to the probe-attached Pc, because there are lysine residues on both sides of the complex. It was assumed in the initial experiments that cytb_6f complexes tethered with their stromal face distal to the surface, thus with a hidden Pc binding site, would not interact with the Pc probe.

To investigate the influence of cytb_6f orientation we tested native grana membranes, where the cytb_6f complexes have a single uniform orientation that favours the formation of an ET complex. We performed measurements on grana membranes prepared for AFM imaging as previously described [24] under exactly the same conditions used for the surface-immobilised cytb_6f and using the same AFM probes functionalised with pre-oxidised Pc, except the imaging buffer contained divalent Mg^{2+} ions to enhance the immobilisation of the grana membrane to the substrate. Simultaneously acquired topographic (Fig. 6A) and adhesion maps (Fig. 6C), were used to quantify the interaction between the cytb_6f in the grana membrane and pre-oxidised Pc on the

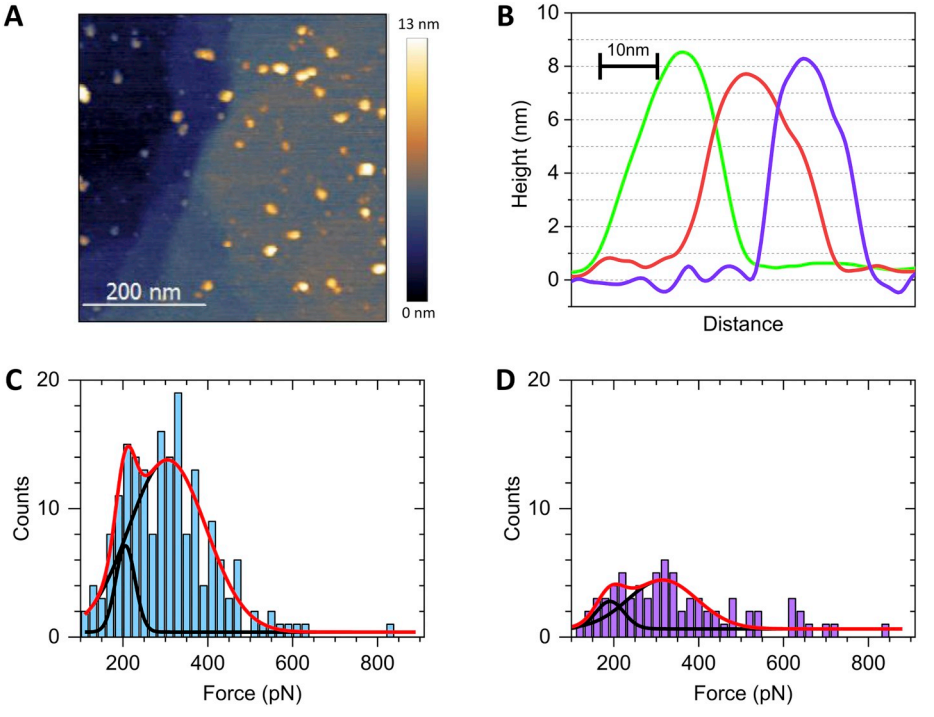

Fig. 5. Single molecule force spectroscopy of the interaction between cytb_6f immobilised on a epitaxial gold surface and Pc attached to the AFM probe. (A) AFM height image showing distribution of cytb_6f complexes on the gold substrate; (B) Height profiles of individual cytb_6f complexes from (A) showing good agreement with the expected height of the complex derived from its structure. (C) Force distribution for the interaction between cytb_6f[red] and Pc[ox] and (D) cytb_6f[red] – Pc[red]. The data in (C) and (D) were normalized by using the surface density of the immobilised cytb_6f complexes on the substrate and assuming uniform distribution of the Pc on the AFM probe. For C and D, the red line on each plot shown the multiple peak fitting gaussian for the plot, and the black lines shows the underlying single peak fits comprising the multipeak fit.

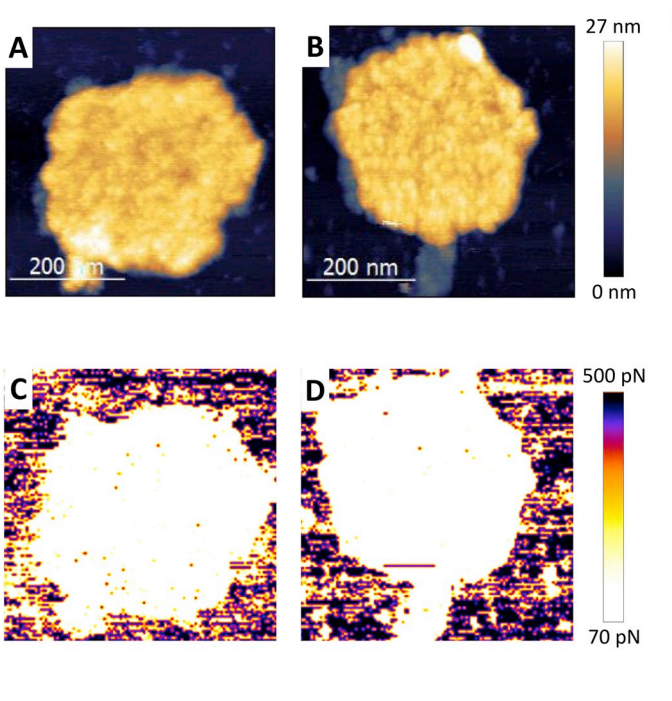

Fig. 6. Single molecule force spectroscopy of the interaction between cytb_6f in spinach grana membranes and Pc attached to the AFM probe. (A) Topographic AFM image of the lumenal side of a native grana membranes from spinach and the corresponding adhesion map in (C), showing the interaction events occurring between Pc[ox] attached to the probe and cytb_6f[red] in the membranes. (B) and (D) Corresponding topography and adhesion images after the grana membrane had been incubated with an excess of Pc[ox] to block the available cytb_6f binding sites. (E) The cumulative interaction frequency for the cytb_6f[red] and Pc[ox] with (blue) and without (red) excess of free oxidised Pc. Error bars show the standard error of the mean. (F) Comparison between the distributions of the unbinding force for cytb_6f[red] and Pc[ox] with (blue) and without (red) an excess of free Pc[ox]. The data in (E) and (F) were normalized by using the estimate number of cytb_6f complexes in the grana and assuming uniform distribution of the Pc on the AFM probe.

AFM tip. In addition, a control measurement was performed, where an excess of free pre-oxidised Pc in the imaging buffer was used to block the docking site on the cytb_6f complex. Comparison of Fig. 6C and D shows a significant decrease in the number of the recorded interaction events in the presence of excess Pc[ox], and statistical analysis of the interaction frequency revealed that excess Pc[ox] caused an expected drop (decrease by a factor of ca. 3, Fig. 6E, F) in the cumulative interaction frequency. Furthermore, there is no indication of a ca. 220 pN peak in the force distribution histogram; the most probable unbinding force was found to be 328 ± 69 pN, in agreement with our results from previous experiments [24]. These findings imply that the presence of second peaks (at lower values of ca. 220 pN) in the unbinding force histograms recorded with surface-immobilised cytb_6f might be related to poor orientation of cytb_6f on the sample substrate.

3. Discussion

We have performed a serial, molecule-by-molecule study of the interaction of Pc with its native electron donor cytb_6f. The parameters obtained in bulk, ensemble studies that would describe such an interaction, such as dissociation constants, have no counterpart at the single molecule level, and instead we obtain binding frequencies and unbinding forces in pN. The behaviour of single molecules, rather than the collective billions studied in bulk measurements, are arguably a valid representation of intermolecular processes that occur in vivo. Our previous AFM study of the Pc-cytb_6f interaction used grana membranes isolated from spinach, adsorbed onto a mica surface [24]. Although native membranes have the advantage of consistently presenting the lumenal face of the cytb_6f complexes to incoming Pc molecules borne on the AFM probe, many thousands of cytb_6f complexes are required for statistical analysis. The present study, which uses purified cytb_6f complexes immobilised on silicon or gold, makes large numbers of molecules available for our PF-QNM approach and records a much larger number of unbinding events within a given scan area compared to cytb_6f in membranes. This approach also ensures that the Pc targets only cytb_6f complexes rather than the heterogeneous surface of a native photosynthetic membrane. However, there is a likely mixed orientation of cytb_6f complexes, arising from lysine attachment points on both the stromal and lumenal faces of the complex, and tethered complexes could pivot around their flexible attachment point on the silicon or gold substrate, presenting a tilted binding site that could lower the frequency of interaction with tip-bound Pc. Nevertheless, our use of purified proteins did produce robust statistics for the unbinding force of ca. 310 pN required to pull apart the cytb_6f – Pc complex. There is good agreement with the previous measurements and those in Fig. 6 in the present work, also on membranes, which yielded ca. 310 pN [24]. Using purified cytb_6f complexes dispersed over a planar surface also yielded a second, lower unbinding force (ca. 220 pN), which we attribute to tilted cytb_6f complexes pivoting about their tether and poorly oriented for presenting the full complement of surface charges on cyt *f* to the tip-

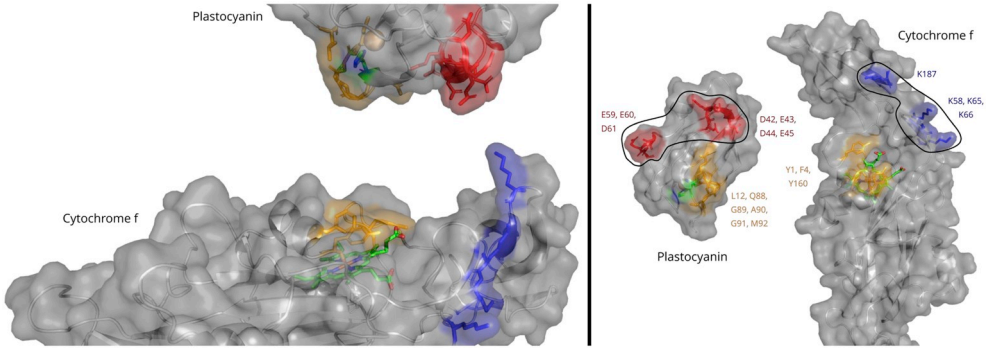

Fig. 7. Binding interface between spinach plastocyanin and cytochrome b_6f. Plastocyanin and cytb_6f binding interfaces shown in Pymol from the plastocyanin structure (pdb:1AG6) and modelled cytochrome *f* structure (Swiss model [28], using cytochrome *f* – Spinach sequence, mapped to structure of C.reinhardtii cytochrome *f* – pdb:1Q90). Acidic residues are highlighted in blue, basic in red and hydrophobic regions are in orange.

attached Pc (see Fig. 7). Such a transient complex might be expected to be easier to separate, when compared with the fully established cytb_6f – Pc ET complex. Also, we cannot exclude the possibility that the ca. 220 pN unbinding force reflects a non-native association of Pc with the stromal surface of cytb_6f complexes tethered in an inverted orientation, e.g. via interaction with a putative ferredoxin binding site.

The use of Pc with its attachment site on the AFM probe distal to the Pc-cyt*f* contact region steers the Pc toward its binding site on cyt *f*. Once brought into contact, the probe tethered Pc and the cytb_6f at the surface have a limited time to form an interaction prior to the retraction of the probe. The Pc docking site on the cytb_6f complex is located on the lumenal domain of cyt *f*. The initial loose electrostatic interaction is guided by a basic patch comprised of K58, K65, K66 and K187 on cyt *f* and two acidic patches on Pc comprised of residues 42–45 and 59–61 [2,15] (Fig. 7). The ionic strength dependence of the interaction frequency shows that this initial electrostatic encounter shows significant screening at 250 mM NaCl, so the physiologically relevant range of 100–200 mM, even to ca. 350 mM [29,33,34] is far from being optimized for cytb_6f-Pc binding. Site-directed mutagenesis of the five lysines comprising the putative Pc binding site of cyt *f* in *Chlamydomonas reinhardtii,* roughly corresponding to the Lys residues highlighted in Fig. 7, had only a limited effect on cyt *f* oxidation, much less than expected from in vitro mutagenesis studies [14,30], so electrostatic forces might not play a large role in mediating encounters between cytb_6f and Pc in vivo.

A kinetic study conducted using recombinant Pc and native cytb_6f complexes from spinach used site directed mutagenesis to alter Pc residues on the face that encounters the lumenal surface of cyt *f*; acidic patches D42, E43, D44, E45 and E59, E60, D61. Y83, A90 and L12 in the flat hydrophobic surface region were also examined, and most of these residues are represented in Fig. 7. This study pointed to an initial encounter where there is a pre-orientation of Pc mediated by transient, long-range electrostatic forces involving the acidic patches of Pc (red in Fig. 7), and complementary basic residues (blue in Fig. 7) in cyt *f* [11]. A more recent study used NMR to study the membrane-bound cytb_6f and Pc from spinach and concluded that hydrophobic interactions (L12, and A90 on Pc and Y1, Y4, Y160 on cyt *f*) form the more tightly bound electron transfer complex [15].

The AFM experiments described in the present study, with probe-attached Pc brought into transient contact with surface-tethered cytb_6f complexes, is intended to measure the forces at the single molecule level that stabilize the ET complex, and to examine the influence of the oxidation/reduction state of the reactants. Thus, the Pc, descending toward a tethered cytb_6f complex must locate its binding site on cytb_6f via translational and rotational movements, guided by loose, complementary electrostatic forces. The ca. 500 μs dwell-time of the AFM probe, longer than the 70–130 μs cytb_6f-Pc ET is sufficient to allow formation of a tight ET complex where the close, hydrophobic contact zone has been established. Our method quantifies the unbinding force, ca. 310 pN, required to disrupt this hydrophobic interaction.

We also measure the interaction frequency, a relative measurement of the formation of the Pc- cytb_6f complex that is indicative of the association rate of the complex. It is the interaction frequency, rather than the unbinding force, that shows a redox dependency; the unbinding forces required to disrupt the interactions between all reduced/oxidised combinations are similar, and it is just the frequency of interaction that changes. Whereas previous bulk phase measurements of the Pc-cytb_6f interaction showed no clear redox dependency [12], our previous single-molecule cytb_6f-Pc study using membranes suggested some selectivity [24]. The present study finds similarly high interaction frequencies for the cytb_6f [red]-Pc[ox] and cytb_6f [ox]-Pc[red] pairs (Fig. 3). Thus, complementary redox states for the cytb_6f and Pc are essential for bringing about a highly probable interaction but once the association is established, likely through short-range hydrophobic contacts, the same level of force is required to disrupt it, regardless of redox states. The PF-QNM experiments therefore show that formation of the docking interface is under redox state control, as also found for the MD simulations of the analogous cyt bc_1 - cyt c_2 interaction [22]. Complementary charges on the cytb_6f and Pc cofactors must contribute to the electrostatic forces that initiate formation of the ET complex. Continued turnover of the cytb_6f complex will regenerate cytb_6f [red] and produce a strongly disfavoured cytb_6f [red]-Pc[red] pair. However, other factors probably contribute to the undocking of Pc[red], including encroaching water molecules destabilising the hydrophobic interface as envisaged for cyt bc_1 - cyt c_2 [22].

The thermodynamic driving force for the cyt c_2- cyt bc_1 and Pc-PSI ET reactions is much larger (100–150 mV) than that for Pc-cytb_6f ET (30 mV, [5]). It therefore seems likely that the small driving force for the cytb_6f to Pc ET prolongs the lifetime of the bound state since the reaction is readily reversible and this could provide an explanation for the relatively slow ET rate (ca. 70-130 μs) compared to that reported for Pc to PSI (ca. 10 μs) [5]. Interestingly however, the interaction frequencies for the cytb_6f [ox]-Pc[*ox*]and cytb_6f [red]-Pc[red] pairs were around 5 times lower (Fig. 3A). Therefore, once the two proteins have dissociated the arrival of another electron on cyt *f* will significantly lower the probability of cytb_6f[red] rebinding the just-reduced Pc molecule. Nature likely uses this phenomenon to avoid 'product inhibition', in other words unproductive encounters between Pc and cytb_6f molecules in the same redox state, ensuring the efficiency and directionality of the electron transport process. Future studies can now focus on testing the roles of specific residues within the binding locus on the unbinding force and interaction frequency.

4. Materials and methods

4.1. Purification of the cytochrome b_6f complex

Spinach was purchased from the local market. Thylakoid membranes were extracted as in Dietrich and Kuhlbrandt [31]. Following this, the membranes were diluted to 2 mg/ml chlorophyll, with a final concentration of 1% 6-O-(N-heptylcarbamoyl)-methyl-α-D-glucopyranoside (HECAMEG) in 40 mM Tricine pH 8.0, 10 $MgCl_2$, 10 mM KCl (Reconstitution buffer) for 3 min. HECAMEG was used for its ability to selectively solubilise cytb_6f [31,32]. The mixture was then diluted 1.4 x and spun at 95,000 x*g* for 30 min. The supernatant was concentrated and applied to a 10–35% sucrose gradient, made in reconstitution buffer, with 0.8% HECAMEG, and centrifuged at 125,000 x*g* for 16 h. The dark band seen in Fig. S2A (left) was taken and loaded onto a 5 ml Ceramic Hydroxyapatite (CHT) column (Bio-Rad) equilibrated in 20 mM Tricine pH 8.0, 25 mM HECAMEG. A wash buffer of 100 mM ammonium phosphate pH 8.0 was then used to remove any green colour. The brown band on the column was then eluted using 400 mM ammonium phosphate. The CHT column product was then placed on another 10–35% sucrose gradient in 50 mM HEPES pH 8.0, 20 mM NaCl, 0.3 mM trans-4-(trans-4′-propylcyclohexyl)cyclohexyl-a-D-maltoside (tPCC-α-M), and centrifuged at 125,000 x*g* for 16 h. The resulting band (S2A, right) was extracted then applied to a Superdex™ 200 FPLC gel filtration column equilibrated in 50 mM HEPES pH 8.0, 20 mM NaCl, 0.2 mM tPCC-α-M. The single peak from the elution was pooled and concentrated down to 66 μM using a Merck™ Centriprep® 50 K Centrifugal filter. Sucrose was added to a final concentration of 10% as a cryoprotectant. This was then frozen at −80 °C until use.

Cytb_6f concentration was measured using an extinction coefficient of 20 mM^{-1} [35] for cytochrome b_6 in dithionite-reduced minus ascorbate-reduced difference spectra.

4.2. Purification of plastocyanin

Spinach leaves were briefly blended in 50 mM sodium phosphate pH 7.4, 5 mM $MgCl_2$, 300 mM sucrose. Following this, leaves were filtered through two layers of muslin cloth, and then repeated through muslin and cotton. The solution was centrifuged for 15 min at 4000 × *g*.

The pellet was resuspended in 10 mM Tricine pH 7.4, 5 mM $MgCl_2$ (Buffer 2) and left on ice for 1 min. This was then diluted 2× with Buffer 2 containing an additional 400 mM sucrose and centrifuged again at 4000 ×*g* for 15 min. The pellet was resuspended to a chlorophyll concentration of 2 mg/ml in 10 mM HEPES pH 7.6, 5 mM NaCl, 5 mM EDTA, and sonicated for 10 min, at 30 s intervals. The solution was then centrifuged at 200,000 x*g* for 1 h to pellet any large unbroken material. The supernatant was then applied to 4 × 5 ml GE Healthcare Hi-TRAP Q FF anion exchange columns chained together, equilibrated in HEPES pH 8, 5 mM NaCl. A gradient of 0.005–1 M NaCl was used for elution, with Pc eluting around 200 mM. Pc-containing fractions were identified by the blue colour upon addition of potassium ferricyanide. These fractions were pooled, concentrated in a Vivaspin 3 kDa cut off spin concentrator, and loaded onto a Superdex™ 200 FPLC column, equilibrated with 20 mM HEPES pH 8, 20 mM NaCl. The resulting Pc fractions were pooled, concentrated, and frozen at −80 °C until use.

4.3. Surface functionalisation

Silicon Wafers and Si/Si_3N_4 AFM probes (Olympus BioLever Mini AC40/Bruker Peakforce-HIRS-SSB) were initially submerged in piranha solution (3:5 *v*/v H_2O_2:H_2SO_4) for an hour to clean and oxidise the Si surface. Following this, both tips and surfaces were cleaned extensively in H_2O, dried under a stream of argon and left in a desiccation chamber overnight under vacuum to remove H_2O from the surface. Tips and surfaces were then placed into another chamber, which had been purged with argon for 10 min. 2 × 15 µl (3-mercaptopropyl)trimethoxysilane (MPTMS) in Eppendorf™ 1.5 ml lids were placed into chamber, followed by another 5 min purge. The chamber was then evacuated and left for ca. 24 h to allow the deposition of the MPTMS self-assembled monolayer. Tips and surfaces were then washed with H_2O to remove any MTPMS not covalently attached to the Si, and dried under a stream of argon. Si wafers were then incubated with 5 mM sulfosuccinimidyl 4-[*N*-maleimidomethyl]cyclohexane-1-carboxylate (SMCC, ThermoFisher Scientific) in linkage buffer (10 mM HEPES pH 7.6) for 45 min, followed by incubation with 700 nM cytb_6f. Surfaces were then washed thoroughly in imaging buffer (10 mM HEPES pH 7.4, 10 mM NaCl, 0.05% GDN (*w*/*v*)) and stored in imaging buffer until use. Tips were incubated with 1 mM (succinimidyl-[(N-maleimidopropionamido)-tetracosaethyleneglycol] ester ($SM(PEG)_{24}$, ThermoFisher Scientific), a ca. 10 nm long linker for 45 min in linkage buffer. Following this they were incubated in 750 nM plastocyanin in 20 mM HEPES pH 7.4, 20 mM NaCl. Tips were then washed in imaging buffer and stored in the same buffer until use.

Epitaxially grown Au [111] thin layers (PHASIS, Switzerland) were functionalised, as received and without further treatment, with mixed EG_3 ((11-Mercaptoundecyl)tri(ethylene glycol), Sigma-Aldrich) and NH_2-thiol (Sigma-Aldrich) mixed at a ratio of 1:200 (mol/mol)/ self-assembled monolayer. Sparse amines were then reacted with dimethyl suberimidate (DMS, ThermoFisher Scientific) for 45 min. Following washing with H_2O the surfaces they were then incubated with 500 nM cytb_6f for 45 min. Surfaces were then washed with imaging buffer and stored in the same buffer until use.

4.4. Atomic force microscopy

Atomic force microscopy and DFS measurements were carried out on a Bruker Multimode 8, using Nanoscope version 9.2. Deflection sensitivities were obtained using a clean Si surface to measure the deflection, whilst the spring constants were determined using Bruker's inbuilt thermal tune function; the obtained spring constants for the cantilevers used were in the range 0.08–0.14 N m^{-1}. Force measurements were taken using the Bruker Peak Force Quantitative Nanomechanical Mapping (PF-QNM) mode, with the peak contact force being kept between 50 and 250 pN. The modulation frequency was kept at 0.5 kHz, with an image size of 128 $pixels^2$, over an area of 500 × 500 nm. Imaging was performed in imaging buffer unless stated otherwise. Reduction of both proteins was achieved by a 15-min incubation with 1 mM sodium ascorbate, and oxidation by the same incubation with potassium ferricyanide. For redox states; a baseline experiment was performed, placing both proteins in the pre-ET state (cytb_6f [red]-Pc[ox]), and 5 images were taken using these conditions. The probe and tip were then re-incubated in the conditions given by the experiment, and further images were obtained. As a result, the adjusted frequencies represent a comparison of the new condition to the pre-ET state, as such the pre-ET state itself has an adjusted frequency of 1 (Fig. 3A). For salt concentrations, a similar baseline was taken however for 5 mM NaCl, and images obtained at other salt concentrations using the same tip were adjusted as such. In addition, the order of these was also changed, so that 5 mM NaCl was not always the first experiment performed but was always included to allow the adjusted frequency to be calculated. Performing the experiments in different orders was found to have no effect.

4.5. Data processing

All the AFM data was analysed by using Gwyddion v 2.51 (open source software covered by GNU general public license, www.gwyddion.net), Nanoscope Analysis v 1.80 (Bruker), MATLAB 2017a and OriginPro 2016 (OriginLab Corp.) software. Analysis of force curves was performed using a homemade MATLAB script, utilising Bruker's Nanoscope MATLAB tools to open the files directly, and display each force curve that met predetermined parameters**. Manual data selection from these force curves was then performed via MATLAB GUI. The extracted data was then analysed in Origin. The most probable values for the unbinding forces were obtained from the maximum of the Gaussian fit to the force distribution combined in a statistical histogram. **Data reduction (positive identification of specific rupture events) was based on the identification of rupture events greater than 90pN (for initial experiments, later raised to 150pN), and occurring at tip-sample separation in the range 5–50 nm; all force-distance curves not exhibiting these properties were not pre-selected for further review.

4.6. Membrane purification

Spinach grana membranes were prepared for AFM imaging according to Johnson et al., [24].

Transparency document

The Transparency document associated with this article can be found, in online version.

Acknowledgments

M.P.J. and C.N.H gratefully acknowledge funding (BB/M000265/1 and BB/P002005/1) from the Biotechnology and Biological Sciences Research Council (U.K.). C.N.H. also acknowledges financial support from Advanced Award 338895 from the European Research Council. G.E.M. was supported by a doctoral studentship from The Grantham Foundation. This work was also supported as part of the Photosynthetic Antenna Research Center (PARC), an Energy Frontier Research Center funded by the US Department of Energy, Office of Science, and Office of Basic Energy Sciences under Award Number DE-SC0001035. PARC's role was to partially fund the Multimode VIII AFM system and to provide partial support for C.N.H.

Appendix A. Supplementary data

Supplementary data to this article can be found online at https://doi.org/10.1016/j.bbabio.2019.06.013.

References

[1] C.C. Moser, C.C. Page, R. Farid, P.L. Dutton, Biological Electron Transfer, J. Bioenerg. Biomembr. 27 (1995) 263–274.
[2] A.B. Hope, Electron transfers amongst cytochrome f, plastocyanin and photosystem I: kinetics and mechanisms, Biochim. Biophys. Acta 1456 (2000) 5–26.
[3] M. Ubbink, The courtship of proteins: understanding the encounter complex, FEBS Lett. 583 (2009) 1060–1066.
[4] E.L. Gross, Plastocyanin: structure and function, Photosynth. Res. 37 (1993) 103–116.
[5] W. Haehnel, A. Pröpper, H. Krause, Evidence for complexed plastocyanin as the immediate electron donor of P-700, BBA - Bioenerg. 593 (1980) 384–399.
[6] W. Haehnel, Photosynthetic electron transport in higher plants, Annu. Rev. Plant Physiol. 35 (1984) 659–693.
[7] H. Kirchhoff, C. Hall, M. Wood, M. Herbstova, O. Tsabari, R. Nevo, D. Charuvi, E. Shimoni, Z. Reich, Dynamic control of protein diffusion within the granal thylakoid lumen, Proc. Natl. Acad. Sci. 108 (2011) 20248–20253.
[8] X.S. Gong, J.Q. Wen, N.E. Fisher, S. Young, C.J. Howe, D.S. Bendall, J.C. Gray, The role of individual lysine residues in the basic patch on turnip cytochrome f for electrostatic interactions with plastocyanin in vitro, Eur. J. Biochem. 267 (2000) 3461–3468.
[9] S.E. Hart, B.G. Schlarb-Ridley, C. Delon, D.S. Bendall, C.J. Howe, Role of charges on cytochrome f from the cyanobacterium Phormidium laminosum in its interaction with plastocyanin, Biochemistry 42 (2003) 4829–4836.
[10] B. Hyun Lee, T. Hibino, T. Takabe, P.J. Weisbeek, T. Takabe, Site-directed mutagenetic study on the role of negative patches on silene plastocyanin in the interactions with cytochrome f and photosystem I, J. Biochem. 117 (1995) 1209–1217.
[11] J. Illerhaus, L. Altschmied, J. Reichert, E. Zak, R.G. Herrmann, W. Haehnel, Dynamic interaction of plastocyanin with the cytochrome b6f complex, J. Biol. Chem. 275 (2000) 17590–17595.
[12] S. Modi, M. Nordling, L.G. Lundberg, Ö. Hansson, D.S. Bendall, Reactivity of cytochromes c and F with mutant forms of spinach plastocyanin, BBA - Bioenerg. 1102 (1992) 85–90.
[13] K. Sigfridsson, Plastocyanin, an electron-transfer protein, Photosynth. Res. 57 (1998) 1–28.
[14] G.M. Soriano, M.V. Ponamarev, G.S. Tae, W.A. Cramer, Effect of the interdomain basic region of cytochrome f on its redox reactions in vivo, Biochemistry 35 (1996) 14590–14598.
[15] T. Ueda, N. Nomoto, M. Koga, H. Ogasa, Y. Ogawa, M. Matsumoto, P. Stampoulis, K. Sode, H. Terasawa, I. Shimada, Structural basis of efficient electron transport between photosynthetic membrane proteins and plastocyanin in spinach revealed using nuclear magnetic resonance, Plant Cell 24 (2012) 4173–4186.
[16] T.E. Meyer, Z.G. Zhao, M. a Cusanovich, G. Tollin, Transient kinetics of electron transfer from a variety of c-type cytochromes to plastocyanin, Biochemistry 32 (1993) 4552–4559.
[17] L. Qin, N.M. Kostić, Importance of protein rearrangement in the electron-transfer reaction between the physiological partners cytochrome f and plastocyanin, Biochemistry 32 (1993) 6073–6080.
[18] P.B. Crowley, N. Vintonenko, G.S. Bullerjahn, M. Ubbink, Plastocyanin-cytochrome f interactions: the influence of hydrophobic patch mutations studied by NMR spectroscopy, Biochemistry 41 (2002) 15698–15705.
[19] M. Ubbink, D.S. Bendall, Complex of plastocyanin and cytochrome c characterized by NMR chemical shift analysis, Biochemistry 36 (1997) 6326–6335.
[20] A.N. Volkov, D. Ferrari, J.A.R. Worrall, M. Ubbink, W. Reinle, R. Bernhardt, M. Ubbink, The orientations of cytochrome c in the highly dynamic complex with cytochrome b5 visualized by NMR and docking using HADDOCK, Protein Sci. 14 (2005) 799–811.
[21] J.A.R. Worrall, Y. Liu, P.B. Crowley, J.M. Nocek, B.M. Hoffman, M. Ubbink, Myoglobin and cytochrome b5: a nuclear magnetic resonance study of a highly dynamic protein complex, Biochemistry 41 (2002) 11721–11730.
[22] A. Singharoy, A.M. Barragan, S. Thangapandian, Binding Site Recognition and Docking Dynamics of a Single Electron Transport Protein : Revisiting Cytochrome c 2, (2016), pp. 1–37.
[23] C. Vasilev, A. a Brindley, J.D. Olsen, R.G. Saer, J.T. Beatty, C.N. Hunter, Nanomechanical mapping of the interactions between surface-bound RC-LH1-PufX core complexes and cytochrome c 2 attached to an AFM probe, Photosynth. Res. 120 (2013) 169–180.
[24] M.P. Johnson, C. Vasilev, J.D. Olsen, C.N. Hunter, Nanodomains of cytochrome b 6 f and photosystem II complexes in spinach grana thylakoid membranes, Plant Cell 26 (2014) 3051–3061.
[25] Y. Xue, M. Okvist, O. Hansson, S. Young, Crystal structure of spinach plastocyanin at 1.7 A resolution, Protein Sci. 7 (1998) 2099–2105.
[26] D. Stroebel, Y. Choquet, J.-L. Popot, D. Picot, An atypical haem in the cytochrome b (6)f complex, Nature 426 (2003) 413–418.
[27] R. Delosme, Electron transfer from cytochrome f to photosystem I in green algae, Photosynth. Res. 29 (1) (1991) 45–54.
[28] A. Waterhouse, M. Bertoni, S. Bienert, G. Studer, G. Tauriello, R. Gumienny, F.T. Heer, T.A.P. de Beer, C. Rempfer, L. Bordoli, R. Lepore, T. Schwede, SWISS-MODEL: homology modelling of protein structures and complexes, Nucleic Acids Res. 46 (W1) (2018) W296–W303.
[29] W.M. Kaiser, H. Weber, M. Sauer, Photosynthetic capacity, osmotic response and solute content of leaves and chloroplasts from *Spinacia oleracea* under salt stress, Z. Pflanzenphysiol. 113 (1983) 15–27.
[30] G.M. Soriano, M.V. Ponamarev, R.A. Piskorowski, W.A. Cramer, Identification of the basic residues of cytochrome f responsible for electrostatic docking interactions with plastocyanin in vitro: relevance to the electron transfer reaction in vivo, Biochemistry 37 (1998) 15120–15128.
[31] J. Dietrich, W. Kuhlbrandt, Purification and two-dimensional crystallization of highly active cytochrome b6f complex from spinach, FEBS Lett. 463 (1999) 97–102.
[32] Y. Pierre, C. Breyton, D. Kramer, J.-L. Popot, Purification and characterization of the cytochrome b6f complex from chlamydomonas reinhardtii, J. Biol. Chem. 270 (49) (1995) 29342–29349.
[33] S. Izawa, N.E. Good, Effect of Salts and Electron Transport on the Conformation of Isolated Chloroplasts. I. Electron Microscopy, Plant Physiol. 41 (1966) 544–552.
[34] L.A Staehelin, Reversible particle movements associated with unstacking and restacking of chloroplast membranes *in vitro*, J. Cell Biol. 71 (1976) 136–158.
[35] C. Breyton, C. Tribet, J. Olive, J.-P. Dubacq, J.-L. Popot, Dimer to monomer conversion of the cytochrome b_6f complex. Causes and consequences, J. Biol. Chem. 272 (1997) 21892–21900.